Check for updates

Received: 22 September 2020 | Revised: 19 February 2021 | Accepted: 22 February 2021

DOI: 10.1111/cmi.13322

RESEARCH ARTICLE

WILEY

NS1-mediated upregulation of ZDHHC22 acyltransferase in influenza a virus infected cells

Mohamed Rasheed Gadalla[1,2] | Eliot Morrison[3] | Marina V. Serebryakova[4] | Xueijiao Han[1] | Thorsten Wolff[5] | Christian Freund[3] | Larisa Kordyukova[4] | Michael Veit[1]

[1]Institute of Virology, Free University Berlin, Berlin, Germany

[2]Department of Virology, Faculty of Veterinary Medicine, Cairo University, Giza, Egypt

[3]Institute of Chemistry and Biochemistry, Free University Berlin, Berlin, Germany

[4]A.N. Belozersky Institute of Physico-Chemical Biology, Lomonosov Moscow State University, Moscow, Russian Federation

[5]Unit 17: Influenza and Other Respiratory Viruses, Robert Koch Institute, Berlin, Germany

Correspondence
Michael Veit, Institute of Virology, Free University Berlin, Berlin 14163, Germany.
Email: mveit@zedat.fu-berlin.de

Funding information
Deutsche Forschungsgemeinschaft, Grant/Award Numbers: TRR 186 (278001972), TransRegio 84-B2, Ve 141/18-1; Russian Foundation for Basic Research, Grant/Award Number: 20-54-12007

Abstract

Influenza A viruses contain two S-acylated proteins, the ion channel M2 and the glycoprotein hemagglutinin (HA). Acylation of the latter is essential for virus replication. Here we analysed the expression of each of the 23 members of the family of ZDHHC acyltransferases in human airway cells, the site of virus replication. RT-PCR revealed that every ZDHHC acyltransferase (except ZDHHC19) is expressed in A549 and Calu cells. Interestingly, expression of one ZDHHC, ZDHHC22, is upregulated in virus-infected cells; this effect is more pronounced after infection with an avian compared to a human virus strain. The viral protein NS1 triggers ZDHHC22 expression in transfected cells, whereas recombinant viruses lacking a functional NS1 gene did not cause ZDHHC22 upregulation. CRISPR/Cas9 technology was then used to knock-out the ZDHHC22 gene in A549 cells. However, acylation of M2 and HA was not reduced, as analysed for intracellular HA and M2 and the stoichiometry of S-acylation of HA incorporated into virus particles did not change according to MALDI-TOF mass spectrometry analysis. Comparative mass spectrometry of palmitoylated proteins in wt and ΔZDHHC22 cells identified 25 potential substrates of ZDHHC22 which might be involved in virus replication.

KEYWORDS
acylation, Hemagglutinin, influenza, mass spectrometry, ZDHHC

1 | INTRODUCTION

Hemagglutinin of Influenza A virus is a type I transmembrane glycoprotein with a large ectodomain, a single transmembrane region and a short cytoplasmic tail (Gamblin et al., 2020). HA is acylated with different fatty acids at three highly conserved cysteines. Two are located in the cytoplasmic tail and are exclusively acylated with palmitate; the third is located at the end of the transmembrane region and is acylated with stearic acid (Brett et al., 2014; Kordyukova, Serebryakova, Baratova, & Veit, 2009). These hydrophobic modifications are crucial for virus replication, as demonstrated by the observation that virus mutants lacking more than one acylation site showed either a significant decrease in virus growth or could not be rescued at all by reverse genetics (Chen, Takeda, & Lamb, 2005; Siche et al., 2015; Wagner, Herwig, Azzouz, & Klenk, 2005; Zurcher, Luo, & Palese, 1994).

Influenza A virus contains another palmitoylated protein, the proton channel M2, which is modified by fatty acids at a cysteine located in an amphiphilic helix that has been proposed to mediate the budding

This is an open access article under the terms of the Creative Commons Attribution-NonCommercial-NoDerivs License, which permits use and distribution in any medium, provided the original work is properly cited, the use is non-commercial and no modifications or adaptations are made.
© 2021 The Authors. *Cellular Microbiology* published by John Wiley & Sons Ltd.

of virus particles (Rossman, Jing, Leser, & Lamb, 2010; Sugrue, Belshe, & Hay, 1990; Veit, Klenk, Kendal, & Rott, 1991). Virus mutants with deleted acylation sites revealed no growth defect in cell culture, even if it was exchanged simultaneously with a cholesterol-binding site (Castrucci et al., 1997; Grantham et al., 2009; Thaa et al., 2012). However, acylation of HA and M2 work synergistically with each other, and recombinant viruses with non-acylated M2 are modestly attenuated in mice, indicating that acylation has a beneficial effect for virus replication in vivo (Grantham et al., 2009; Veit & Siche, 2015).

Palmitoylation is catalysed by a family of protein acyltransferases known as the ZDHHC family, a group of polytopic membrane proteins containing an Asp-His-His-Cys (DHHC) motif as the catalytic center in one of their cytoplasmic domains. The DHHC-motif is embedded within a cysteine-rich domain (CRD) that is a variant of the zinc finger motif. Twenty-three ZDHHC proteins are expressed in humans, and each show distinct, but overlapping, substrate specificities (Chamberlain & Shipston, 2015; Zaballa & van der Goot, 2018). Most ZDHHC proteins are abundant in many tissues, but some are expressed in only a few cell types. The majority of ZDHHC proteins localise to Golgi membranes, while smaller numbers are found in the endoplasmic reticulum (ER) or are targeted to the plasma membrane (Ernst et al., 2018; Ohno, Kihara, Sano, & Igarashi, 2006). Besides the cysteine-rich domain, little sequence conservation occurs between proteins. It thus might be feasible to develop small molecules that specifically target only one or a few ZDHHCs, and this development might be facilitated by the recently resolved 3D structures of two ZDHHCs (Rana et al., 2018). Small molecules targeting certain ZDHHCs might be promising antiviral drugs, if they inhibit a modification essential for virus replication while not perturbing acylation of most cellular proteins (Gadalla & Veit, 2019).

We have recently shown that acylation of M2 and HA was greatly reduced if the genes encoding ZDHHC2, 8, 15 and 20 were inactivated by CRISPR/Cas9 (Gadalla, Abrami, van der Goot, & Veit, 2020). This was demonstrated in HAP1 cells, a human leukaemia cell line having only a single copy of almost every chromosome and hence ideally suited for the CRISPR/Cas9 technology. Following this, we were interested to determine which ZDHHCs are present in human lung cells, the original site of Influenza virus replication, and whether tissue-specific expression patterns of ZDHHCs change upon virus infection.

The viral NS1 protein is one of the key virulence factors of the Influenza A virus. It inhibits various cellular processes, mostly in order to impair the innate immune response of the host (Hrincius et al., 2014; Klemm, Boergeling, Ludwig, & Ehrhardt, 2017; Krug, 2015; Schneider & Wolff, 2009). NS1's antagonising effects range from inhibiting intracellular virus sensors and signalling pathways to impairing mRNA processing, export, and translation. In addition, it has been recently shown that NS1 produces dynamic changes in the three-dimensional organisation of the host genome, where it induces read through transcription of hundreds of kilobases at the end of highly transcribed genes via inhibition of transcription termination. The activity of NS1 is a consequence of inhibiting the poly(A) sensing (PAS) subunit of the cleavage and polyadenylation specificity factor CPSF30. Whether this massive upregulation of cellular genes has an effect on influenza virus replication is not known (Heinz et al., 2018).

We show here that NS1 induces the upregulation of one palmitoyl acyltransferase, ZDHHC22, in virus-infected human lung cell lines. While ZDHHC22 is apparently not required for acylation of HA and M2, we nevertheless were able to identify 25 putative cellular substrates of this enzyme by quantitative mass spectrometry.

2 | RESULTS

2.1 | All members of the ZDHHC family (except ZDHHC19) are expressed in human lung cells

We first analysed the expression pattern of members of the ZDHHC palmitoyl acyltransferase family in the human lung cell line **A 549**. This is of interest as many viral pathogens that infect via the respiratory route contain at least one acylated membrane protein, yet the responsible ZDHHCs have only been identified for HA of the Influenza A virus (Gadalla et al., 2020). We designed primer pairs for RT-PCR in such a manner that each primer binds to a different exon to ensure that amplified gene fragments are derived from the mRNA, not from the genomic DNA (Table S1). Agarose electrophoresis of the resulting products from RNA isolated from uninfected cells showed a band of the expected size for most ZDHHCs, except ZDHHC15 and 19 (Figure S1). Note, however, that we later detected ZDHHC15 (but not ZDHHC19) by qPCR.

To evaluate whether the same ZDHHC expression pattern exists in native human lung cells, we consulted the Human Protein Atlas (https://www.proteinatlas.org/), a database that maps global expression patterns of proteins in human cells, tissues and organs using integration of various "Omics" technologies. From the ZDHHCs quantified by mass spectrometry, only ZDHHC8 was not detected in various tissues of the respiratory tract (nasopharynx, bronchus and lung). However, expression of ZDHHC8 was detected by RNAseq at fairly high levels in bulk lung tissue. The only ZDHHCs not detected by RNAseq are ZDHHC22 and ZDHHC19, the latter of which being consistent with our RT-PCR and qPCR-based observations. Note also that substantial differences exist in the ZDHHC expression levels between epithelial cells in the upper respiratory tract (nasopharynx and bronchus) versus pneumocytes and macrophages in the lung (Table S2).

Since infected cells express high levels of HA, which must be fully acylated to function properly, and since most ZDHHCs are present only at a low copy number (Zaballa & van der Goot, 2018), we asked whether the influenza virus might induce overexpression of certain ZDHHCs upon infection. We infected A549 cells with the "human" virus WSN (H1N1) at an MOI of 1. RNA was extracted 5 hr post infection from both infected and uninfected cells, reverse transcribed to cDNA, and relative expression of ZDHHCs was analysed by qPCR (primers are listed in Table S3). Calculation of the mRNA changes upon infection revealed that one ZDHHC gene, *ZDHHC22*, was upregulated fivefold (Figure 1a). Upregulation of *ZDHHC22* was even higher (25-fold) if A549 cells were infected with a variant of avian fowl plaque virus (FPV M1, H7N1 [Wagner et al., 2013]) (Figure 1b). We performed the same experiment with another human lung cell line (Calu-3 cells) which also revealed significant upregulation of

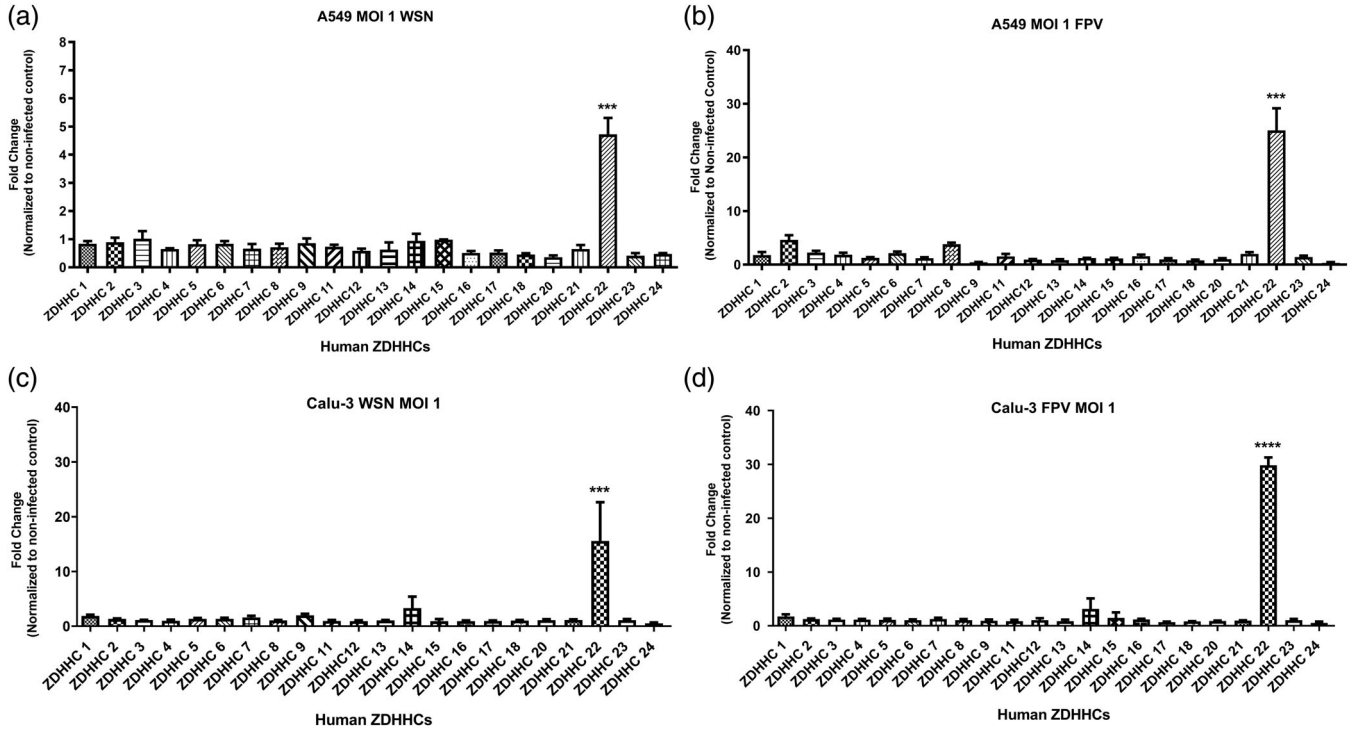

FIGURE 1 ZDHHC22 is upregulated by IAV infection in A549 and Calu-3 cells. A549 cells (a, b) or Calu-3 cells (c, d) were mock infected or infected with WSN (a,c) or with the M1 mutant of FPV (b, d) with an MOI of 1 for 5 hr. Total RNA was isolated, reverse transcribed to cDNA and qPCR was performed to determine the expression of different ZDHHCs. To calculate the fold change of expression of each ZDHHC gene (infected compared to non-infected control), Ct-values of the GAPDH housekeeping gene were subtracted from the Ct-value of each ZDHHC gene and then the relative expression levels displayed as fold change were calculated using the Livak method ($2^{-\Delta\Delta CT}$) (Livak & Schmittgen, 2001). Shown is the mean including standard deviation from three independent experiments. Note that expression of ZDHHC15, but not ZDHHC19, was detected by qPCR. Two-way ANOVA followed by Bonferroni's multiple comparison test was applied on delta CT values for statistical analysis. The asterisks indicate statistically significant differences (***$p < .005$, ***$p < .0001$) between mock and virus infected cells

ZDHHC22. The calculated fold changes were even higher (15-fold) if the Calu-3 cells were infected, with WSN virus and 30-fold if infected with FPV M1 (Figure 1c,d). The exact values of the fold changes for each ZDHHC (mean of three experiments) are depicted in Table S4). Note also that the qPCR analysis further confirmed that Calu-3 cells, like A549 cells, also express every ZDHHC gene except ZDHHC19.

We next analysed expression of ZDHHC22 at different times points after infection with FPV M1. In A549 cells, upregulation of ZDHHC22 was first detected at 3 hr p. i., was elevated several fold at 5 h p. i. and increased further at 7, 9 and 12 hr p. i. In Calu-3 cells upregulation was first evident at 5 hr p. i., but is much more prominent at 9 and 12 hr post infection (Figure S2). This is consistent with the observation that the expression of NS1 increases during the course of virus replication (Kummer et al., 2014).

2.2 | Influenza virus protein NS1 induces upregulation of ZDHHC22 expression

NS1 is the key protein of the influenza virus that modulates the host's innate immune response to infection. In addition, NS1 causes read-through transcription at the end of highly transcribed cellular genes, leading to the expression of several hundred additional genes. The mechanism is likely to involve inhibition of polyadenylation signal (PAS)-dependent transcription termination as a consequence of the binding of NS1 to the polyadenylation-sensing subunit of CPSF30 (Heinz et al., 2018). Thus, we hypothesized that NS1 might be also responsible for the induction of ZDHHC22 upregulation. To test this, we transfected A549 cells with NS1-encoding plasmids from three different influenza strains: from WSN and FPV, but also from the human strain PR8 (Puerto Rico/8/1934, H1N1), which is closely related to WSN but does not bind to CPSF30. qPCR analysis revealed that all NS1 proteins induced expression of ZDHHC22, but to different extents (Figure 2a). FPV-NS1 had the strongest effect; it increased expression of ZDHHC22 by about sixfold, while NS1 of WSN and PR8 caused a threefold upregulation. This corresponds to the effect seen in virus-infected cells, where avian FPV M1 induced a higher upregulation compared to WSN. Western-blotting of cell lysates revealed that NS1 proteins from the human viruses WSN and PR8 are expressed at similar levels, However, the antibody does not recognise NS1 from FPV M1 and thus we cannot exclude completely that the stronger effect of avian NS1 is due to a higher expression level.

We next validated the specificity of NS1-induced upregulation of ZDHHC22 using an available PR8 virus mutant deficient in NS1 expression. Whereas PR8 wt infection increased expression of ZDHHC22 fourfold, no change in the expression level of ZDHHC22

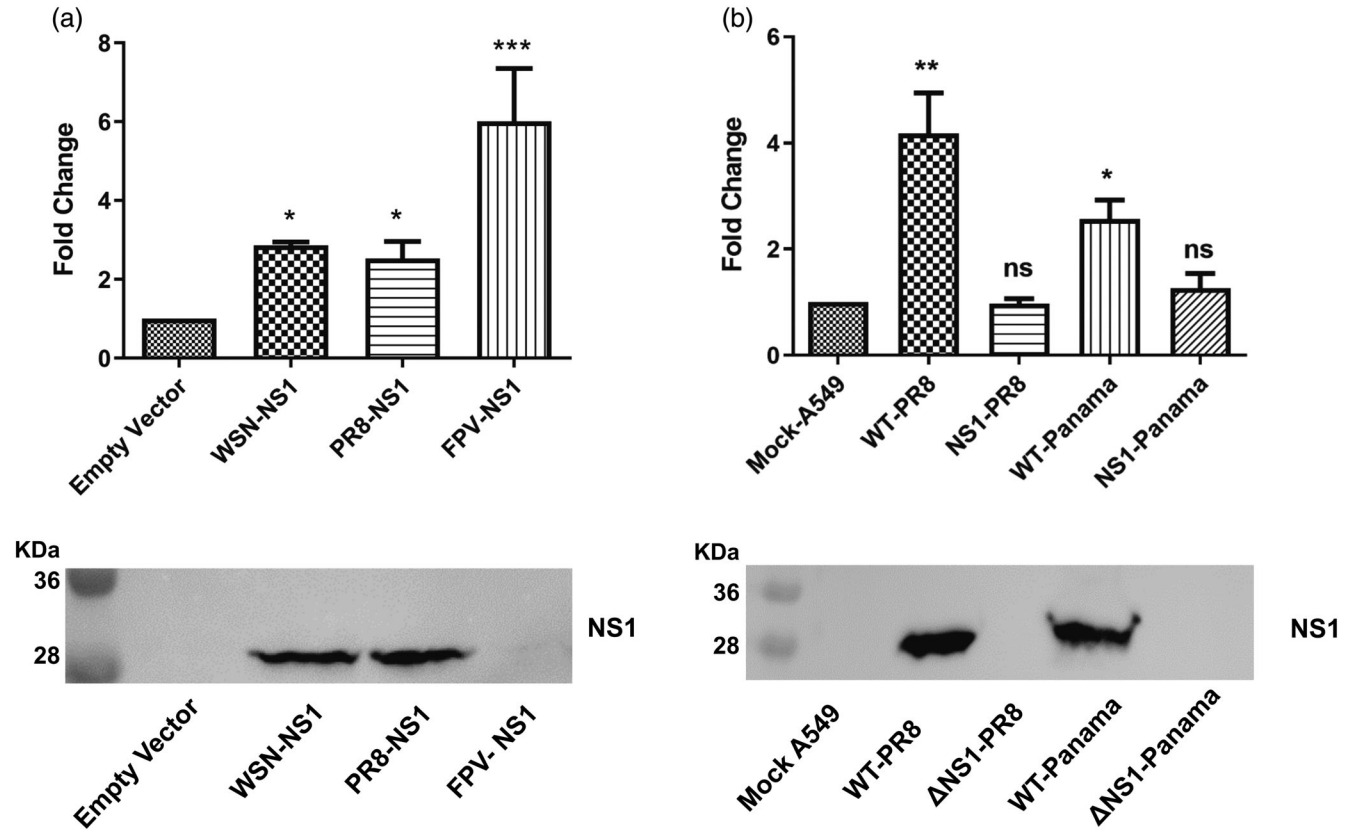

FIGURE 2 Influenza virus NS1 induces upregulation of ZDHHC22. (a) Plasmids encoding NS1 of three different influenza virus strains (WSN, FPV and PR8) or the empty pCAGGS vector were used for transfection of A549 cells. Twenty-four hours post-transfection total RNA was isolated and the fold-change of expression of ZDHHC22 gene was determined as described in Figure 1. Expression data are normalised to empty vector control and results are shown as the mean of three transfections including standard deviation. The asterisks indicate statistically significant differences (*p < .05, **p < .001, ***p < .0005) between mock and transfected/infected cells. One-way ANOVA followed by Tukey's multiple comparison test was applied for statistical analysis. ns, not significant. The lower part shows a western-blot of a cellular lysate prepared at 24 hr post transfection using a monoclonal antibody against the NS1 protein. (b) A549 cells were infected with an MOI of 1 with PR8 or Panama virus, either wild-type or mutant viruses with deletions in the NS1 gene. Five hours post infection total RNA was isolated and the fold-change of expression of ZDHHC22 gene was determined as described in Figure 1. Expression data are normalised to non-infected cells and results are shown as the mean of three infections including standard deviation. The mean ± standard deviation is shown. The asterisks indicate statistically significant differences (*p < .05, **p < .001, ***p < .0005) between mock and transfected/infected cells. One-way ANOVA followed by Tukey's multiple comparison test was applied for statistical analysis. ns, not significant. The lower part shows a western-blot of a cellular lysate prepared at 5 hr post transfection using a monoclonal antibody against the NS1 protein

was detected in cells infected with ΔNS1 mutant virus (Figure 2b). We also analysed a more recent human strain, A/Panama/2007/99, which belongs to the H3N2 subtype. This virus also upregulates expression of ZDHHC22 around 2.5-fold, but the corresponding ΔNS1 mutant virus had no effect. Western-blotting showed that NS1 of PR8 and Panama are expressed at similar levels. Together, these results clearly show that NS1 is responsible for the upregulation of ZDHHC22 and that an NS1 protein from an avian virus had a stronger effect than NS1 proteins from human viruses.

2.3 | No effect of ZDHHC22 knockout on palmitoylation of HA and M2 inside cells

Since Influenza virus induced the expression of ZDHHC22 in lung cells, we hypothesized that this enzyme might play a critical role in acylation of HA and/or M2. To test this hypothesis, we aimed to generate a A549 ZDHHC22 knockout cell line using CRISPR/Cas9 technology (Figure 3a). Two guide RNAs (gRNAs) (Table S5) were designed targeting exon-2 of the *ZDHHC22* gene, which encodes the DHHC domain responsible for the catalytic activity of the enzyme. The two gRNAs were cloned into the pRP-418 vector which also encodes the Cas9 nuclease. After transfection, selection and isolation of single cell clones, we screened for the desired mutation. Due to lack of validated antibodies for most members of the ZDHHC family (including ZDHHC22), we relied on genetic approaches on both the DNA and RNA levels to validate the knockout. PCR measurements of genomic DNA revealed a gene fragment of ~700 bp in wild-type (WT) cells, whereas the corresponding fragment is only ~400 bp in a knockout (KO) cell line indicating that it contains the anticipated 248-bp deletion on both chromosomes (Figure 3b). This was confirmed by sequencing of a chromosomal PCR product of the ZDHHC22 gene. Whereas wild-type cells exhibit the expected DNA sequence, the A549 ZDHHC22 knockout cell line contains a deletion

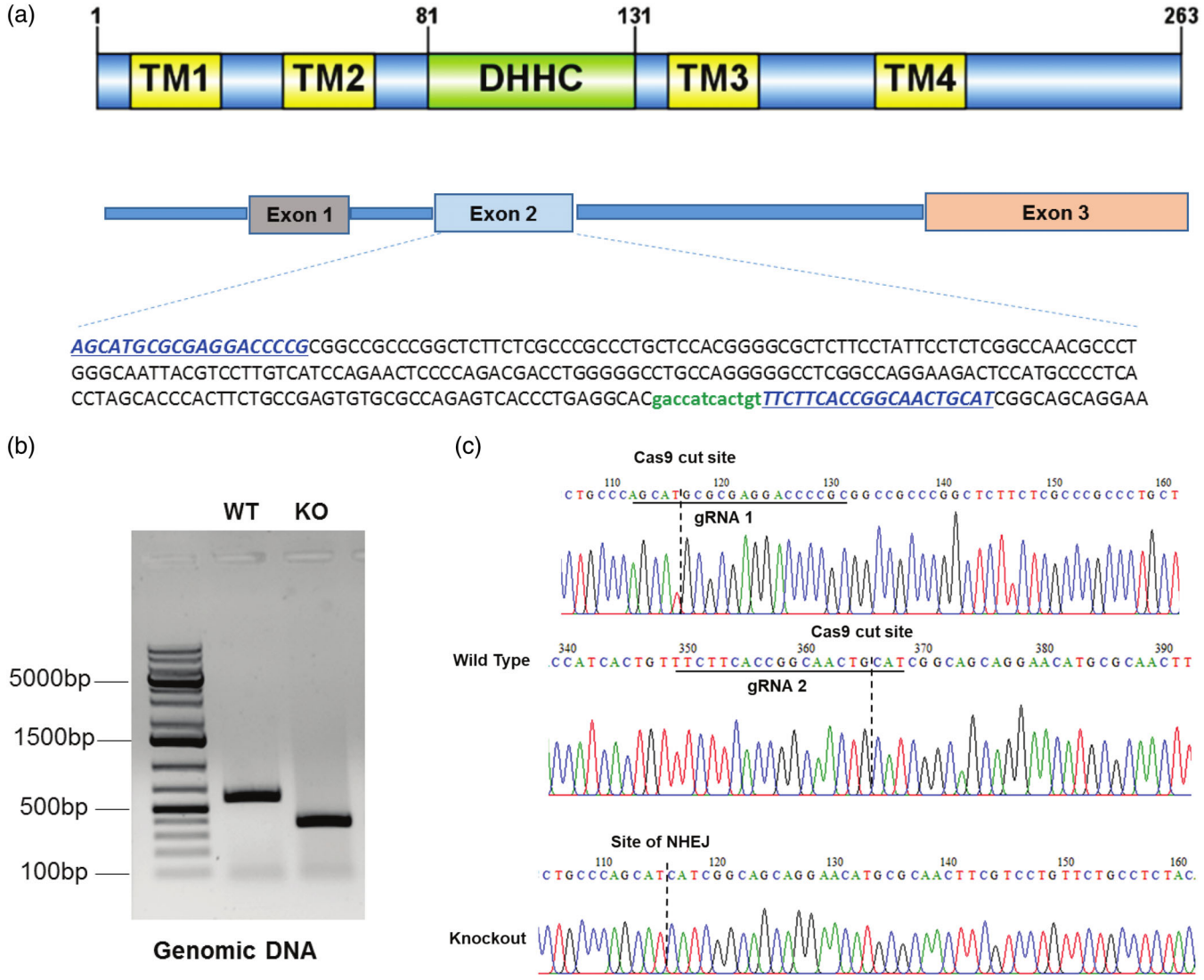

FIGURE 3 Knockout of ZDHHC22 in A549 cells using CRISPR/Cas9. (a) Upper part: Scheme of the human ZDHHC22 protein showing the DHHC motif located between the second and third transmembrane domains (TM2 and TM3). Lower part: Scheme of a region of the gene encoding ZDHHC22. The sequence of exon 2 is shown below. The binding sites of the guide-RNAs are highlighted in blue and the sequence encoding the DHHC motif is highlighted in green. (b) PCR products from genomic DNA (gDNA) isolated from wild type (WT) and knockout cell lines showing biallelic deletion of a ~ 250 bp region in exon-2 of ZDHHC22. (c) Sequencing chromatograms of knockout (KO) and wild type (wt) A549 cells. The binding site of the guide RNA is underlined in the wt sequence. The Cas9 cutting site is indicated by a vertical dotted line. The deletion of 248 bp generates a frameshift in the coding sequence. Parts of the ZDHHC22 gene encompassing the guide RNA binding site were amplified from the genomic DNA by PCR using the primers listed in Table S1

of 248 nucleotides between base positions 116 and 366 (Figure 3c). Since this deletion results in a frameshift in exon-2 it is unlikely that the knockout cells are able to synthesise a functional ZDHHC protein, even if the mRNAs are translated.

Using the ZDHHC22 knock-out cells we first investigated by qPCR whether expression of the other ZDHHC genes was altered relative to wild-type A549 cells. The results revealed that the expression levels of seven ZDHHC genes (1, 7, 8, 9, 13, 20 and 24) remained essentially unchanged. However, many ZDHHC genes were down-regulated; ZDHHCs 2, 3,4, 5, 6, 16, 21 and 23 between ~20% and ~30% and three more clearly, ZDHHCs 11, 14, and 15 by up to 50%. Only two ZDHHC genes were slightly upregulated, ZDHHC12 by ~25% and ZDHHC18 by ~50% (Figure S3). This suggests that ZDHHCs apparently form a complex network; at least the ZDHHC22 gene apparently influences the expression of many other ZDHHC genes.

Having successfully inactivated the *ZDHHC22* gene, we examined palmitoylation of influenza HA using acyl-RAC (resin-assisted capture), a technique that allows the capture of S-acylated proteins on thioreactive sepharose beads (Werno & Chamberlain, 2015). Wt and knock-out cells were infected with WSN virus and lysed, and a 5% aliquot was used to compare the expression levels of HA. One aliquot of the remaining lysate was treated with hydroxylamine to cleave thioester-linked fatty acids, while the other aliquot was treated with

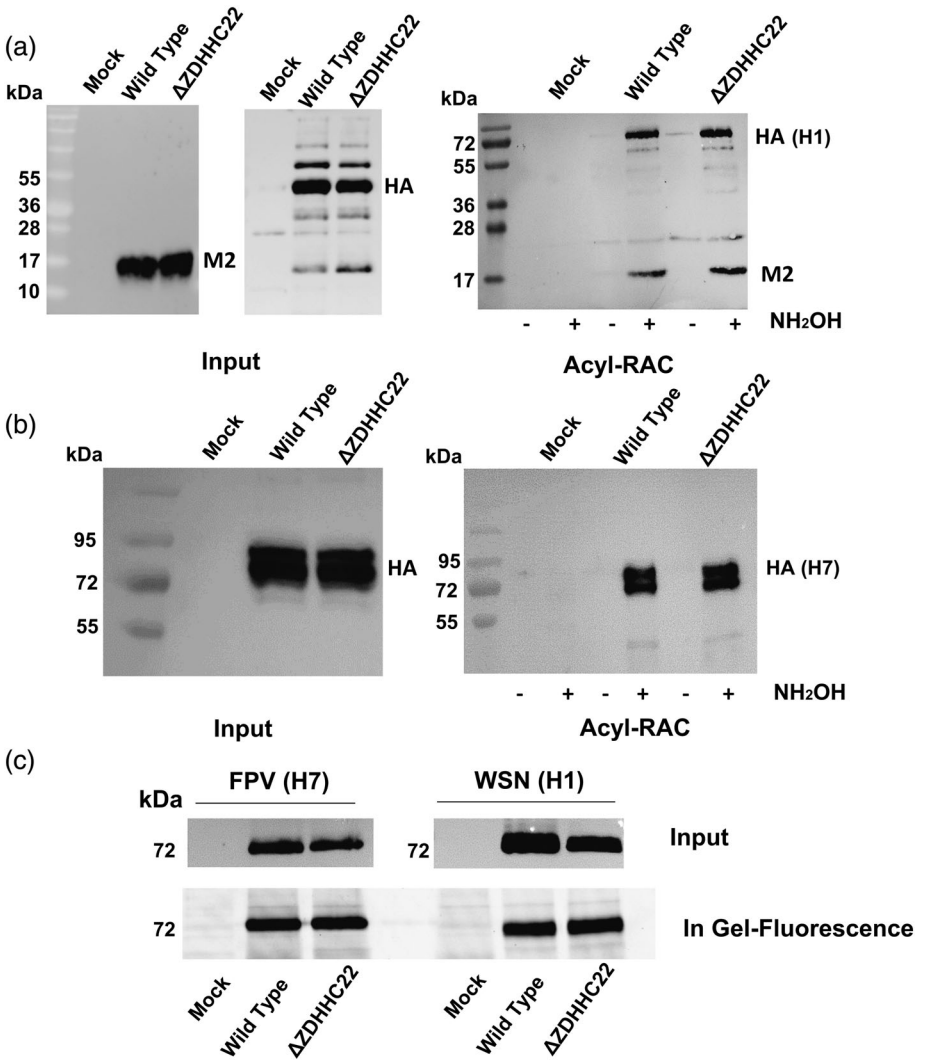

FIGURE 4 Effect of ZDHHC22 knock-out on palmitoylation of influenza virus HA and M2. (a) Wildtype and ΔZDHHC22 A549 cells were infected with a MOI of 1 with WSN virus or were kept uninfected (mock). After 24 hr, cells were lysed and subjected to acyl-RAC and Western blotting. Left, Input: Western blot of 5% of the lysate to check expression levels of HA and M2. Right, acyl-RAC. NH_2OH: samples treated (+) or not treated (–) with hydroxylamine to cleave thioester-bound fatty acids. Both HA and M2 antibodies were used for the same blot membrane. (b) Wildtype and ΔZDHHC22 A549 cells were infected with a MOI of 1 with FPV M1 influenza virus or kept uninfected (mock). After 24 hr, cells were lysed and subjected to acyl-RAC and Western blotting (IB) with antiserum against the HA2 subunit. (c) Wildtype and ΔZDHHC22 A549 cells were infected with an MOI of 1 with WSN or FPV M1 Influenza virus or kept uninfected (mock), as indicated. Cells were labelled 5 hr post infection with the fatty acid analogue 17-ODYA for 6 hr. Viral HA was immunoprecipitated from cellular extracts, 17-ODYA was coupled via click-chemistry to a fluorophore, and the samples were subjected to SDS-PAGE. Gels with fluorescently labelled protein was detected by a 9400 Typhoon scanner

Tris–HCl such that neither cleavage nor bead-binding was expected. Thiol-reactive resins were then added to both aliquots and precipitated proteins were subjected to Western blotting with HA-reactive antiserum. Figure 5a shows that HA is expressed to similar levels and with the same molecular weight in both wt and ZDHHC22 knock-out cells (Figure 5a, input). Most importantly, acyl-RAC revealed that HA is still palmitoylated in ZDHHC22 knock-out cells and apparently to the same extent as in wt cells (Figure 4a, acyl-RAC).

We then investigated whether expression of ZDHHC22 might be upregulated because it catalyses fatty acid attachment to M2, the second palmitoylated protein of Influenza virus. The same blot membrane was treated with M2 antibodies, but the result also showed that M2 is acylated to the same extent in wt and ZDHHC22 knock-out cells (Figure 4a).

As FPV increased the expression of ZDHHC22 to a much larger degree than WSN, we asked whether an effect of this enzyme on acylation of HA might be more pronounced and thus easier to detect. This is also interesting since HA of FPV belongs to the phylogenetic group 2, which might exhibit a different structure in the transmembrane region (containing a putative enzyme recognition motif) than the group 1 HA of WSN. Despite these differences, HA of FPV was seen to be acylated to the same extent in both wt and ΔZDHHC22 cells (Figure 4b).

Acyl-RAC captures HA synthesised at every time point of infection, and thus also before expression of ZDHHC22 is induced. Therefore, we investigated palmitoylation of HA with another method, metabolically labelling with a clickable palmitic acid analogue (17-ODYA) from 5 to 11 hr after virus infection. Immunoprecipitated HA is then coupled to a fluorescent dye (TAMRA-Azide) by click chemistry (Martin, 2013). Visualisation of the fluorescence in an SDS gel revealed that HA of both WSN and FPV M1 were labelled to the same extent in wild type and ΔZDHHC22 cells (Figure 4c).

2.4 | MALDI-TOF shows that HA incorporated into virus particles is fully acylated

It is possible that ZDHHC22 might be specific for stearate or palmitate and in its absence the vacant cysteine is filled by another acyltransferase having another lipid preference. This shift would not

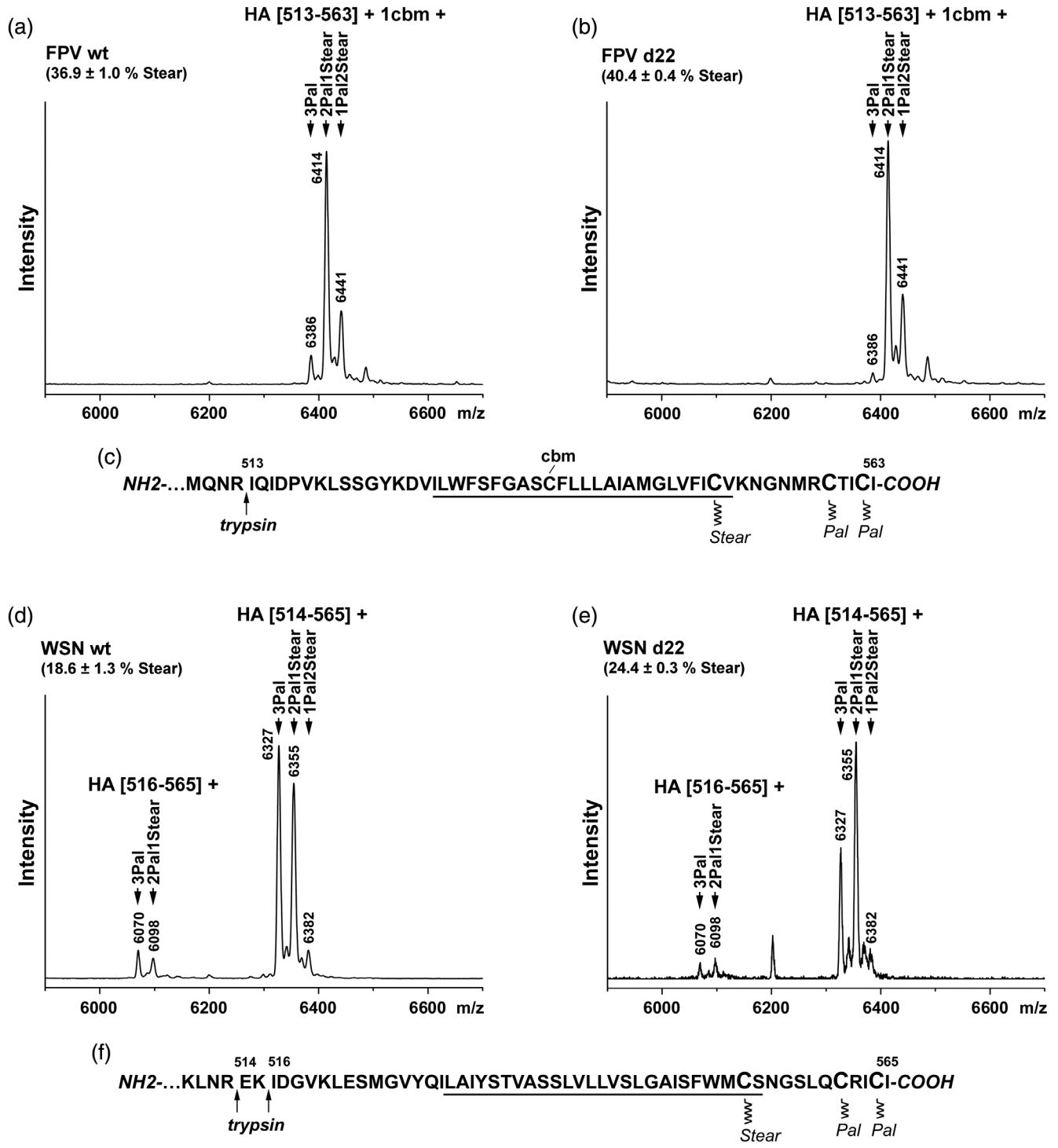

FIGURE 5 MALDI-TOF MS analysis of HA from viruses grown in wild type or ΔZDHHC22 A549 cells. (a, b, d, e) MALDI-TOF MS analysis of HA peptides obtained from FPV M1 (a, b) and WSN (d, e) grown in wt (a, d) or ΔZDHHC22 (b, e) A549 cells. Mass spectra obtained in linear mode are depicted. Indicated are the m/z values of the peaks, the first and the last amino acid residues of the corresponding peptides, mono-carbamidomethylation (cbm; + 57 m/z) of the peptides containing a free cysteine in the middle of TMR and the number and type of HA-bound fatty acids. The stearate amount (+ standard deviation) was calculated for the FPV HA [513–563] and WSN HA [514–565] peptides. Every mass spectrum was obtained as the sum of at least 200 laser shots. Two (WSN wt) or one virus preparation were analysed and at least four mass spectra for every virus sample were recorded and the stearate content was calculated. (c, f) Amino acid sequences of the C-terminal regions of FPV M1 HA (c) and WSN HA (f) indicating the sites of cleavage by trypsin and cysteine modifications. Cysteines that may be potential acylation sites are enlarged and the TMR is underlined. Stear: stearate, Pal: palmitate. The modification of free cysteine located in the middle of FPV HA TMR by a carbamidomethyl group was detected after the reaction with iodoacetamide, as described in Materials and Methods. No mono-carbamidomethylated peptides were detected for WSN HA lacking a free cysteine in the middle of TMR. Importantly, neither double- nor triple-carbamidomethylated peptides were detected for any HA, meaning that no potential acylation sites are free in any HA peptides, but are rather modified with fatty acids

be obvious by the methods thus far described, as neither acyl-RAC nor metabolic labeling can discriminate between the palmitate and stearate attachments. Thus, we used MALDI-TOF mass spectrometry to more quantitatively analyse the fatty acid patterns of HA in virus particles (WSN and FPV M1) prepared from WT and ΔZDHHC22 knockout cell lines (Brett et al., 2014). Pelleted virus particles were treated with iodoacetamide to prevent cysteine-mediated aggregation of proteins that would also reveal free cysteines and thus non- and under-acylated peptides. After separation by non-reducing SDS-PAGE, protein bands were electro-blotted onto membranes and visualised by Ponceau S staining. The band corresponding to HA was cut from the membrane, digested with trypsin, and the resulting peptides were eluted and analysed by MALDI-TOF MS.

HA from FPV M1 grown in wt A549 cells is cut after arginine 512, located 15 amino acids upstream from the TMR, resulting in a peptide that matches to the complete membrane-anchoring plus linker region spanning amino acids 514–563 (Figure 5a,c). The peptide is present as one main peak representing a peptide containing two palmitates and one stearate. In addition, two minor peaks we observed, corresponding to a peptide containing one palmitate and two stearates and a triple palmitoylated peptide. The calculated stearate content is 39.6% (mean of two virus preparations), and thus 10% higher than previously determined for HA of the same virus grown in embryonated eggs. The same pattern of peaks was obtained if FPV M1 was grown in the ΔZDHHC22 cell and the same percentage of stearate was calculated (Figure 5b). Most notably, no peptides with a lower m/z value representing non- or under-acylated peptides (possessing carbamidomethylated instead of S-acylated cysteines) were detected, providing evidence that knocking out ZDHHC22 has no effect on the stoichiometry of S-acylation of HA of FPV meaning that all potential S-acylation sites are occupied.

We then performed the same analysis with HA of WSN virus. Trypsin cuts HA of WSN grown in wt A549 cells mainly after arginine 513, but also after lysine 515 to a lesser extent. Each of the resulting peptides is observed as two main peaks representing a triple palmitoylated peptide and a peptide containing two palmitates and one stearate (Figure 5d,f). The calculated stearate content is 19% and thus slightly lower compared to WSN grown in MDCK cells (23%), but higher if the same virus was grown in embryonated eggs (8%) (Brett et al., 2014). If WSN was grown in ΔZDHHC22 cells the same peptide pattern was observed, only an increase in the stearate content to 24% was calculated. Most importantly, no peaks representing non- or under-acylated peptides were detected (Figure 5e), demonstrating that HA in virus particles is fully acylated.

2.5 | Potential substrates of ZDHHC22 palmitoyl acyltransferase identified by LC–MS/MS

Knockout of *ZDHHC22* did not show any effect on the acylation patterns of either intracellular or virus-incorporated HA. Thus, we hypothesized that NS1 might induce upregulation of ZDHHC22 to acylate cellular proteins. We used acyl-RAC for enrichment of palmitoylated proteins coupled with $^{16}O/^{18}O$-labeling for quantification of the palmitoylome of ΔZDHHC22 cells relative to A549 wild type cells (Morrison et al., 2015). WT and ΔZDHHC22 cells were homogenised and cellular lysates were subjected to the acyl-RAC procedure in the presence of NH_2OH or in its absence (control), followed by binding to thiopropyl sepharose beads. After elution, enriched and control samples were run in parallel lanes of an SDS-PAGE gel. These lanes were horizontally cut into equal-sized bands which were subjected to in-gel trypsin proteolysis in the presence of $H_2{}^{18}O$ ("heavy" water) and $H_2{}^{16}O$ ("light" water) for NH_2OH treated and untreated samples, respectively. This leads to the enzymatic incorporation of one (via hydrolysis of the peptide bond by trypsin) or two (via hydrolysis of the acyl-enzyme complex) ^{18}O isotopes at the C-terminus of peptides from the HA-treated sample. After digestion, samples were mixed and measured by LC–MS/MS; evaluating the isotopic heavy/light intensity ratio gives rise to an enriched pool representing the population of palmitoylated proteins in the cell. Comparing the palmitome of wt with ΔZDHHC22 A549 cells identified 25 proteins in both of the two biological replicates as possible substrates of ZDHHC22 (Table S6), described in more detail below. Quantitative data from this experiment and details about identified proteins, such as their accession numbers and predictions from the SwissPalm database are presented in the Appendix S1.

One of the substrates we identified in this screen is the isoform 1 of plakophilin-2 (PKP-2), which is of interest since it has been described to be palmitoylated and to affect replication of Influenza A virus (Roberts et al., 2014; Wang et al., 2017). The ZDHHCs which acylates PKP-2 has not been identified and it is also not known whether palmitoylation affects the antiviral activity of the protein. We, therefore, aimed to analyse palmitoylation of PKP-2 in ΔZDHHC22 cell. When we performed western blots with total cellular lysates, expression of PKP-2 is barely detectable in knock out cells, although the protein is abundantly expressed both in uninfected and virus-infected wt A549 cells (Figure S4). Furthermore, morphological changes occur in A549 cells during selection of cell clones having an inactivated ZDHHC22 gene. Wt A549 cells are round and are grown to high density 5 days after seeding, whereas ΔZDHHC22 cells remain spindle-shaped and no extensive cell–cell contacts are obvious by light microscopy. Although we could not analyse palmitoylation of PKP-2 in ΔZDHHC22 cells due to its very low expression level, the result is consistent with the function of palmitoylation of PKP-2, which is important for desmosome assembly and hence cell–cell adhesion (Roberts et al., 2014).

2.6 | Growth of influenza virus is not diminished in ΔZDHHC22 cells

Finally, we investigated whether abolishment of ZDHHC22 expression affected virus production. Both wild-type and ΔZDHHC22 cells were infected with FPV M1 or WSN at a low MOI (0.01), supernatants were collected at various time points, and virus titers were determined by plaque assays in MDCK-II cells. Virus titers were

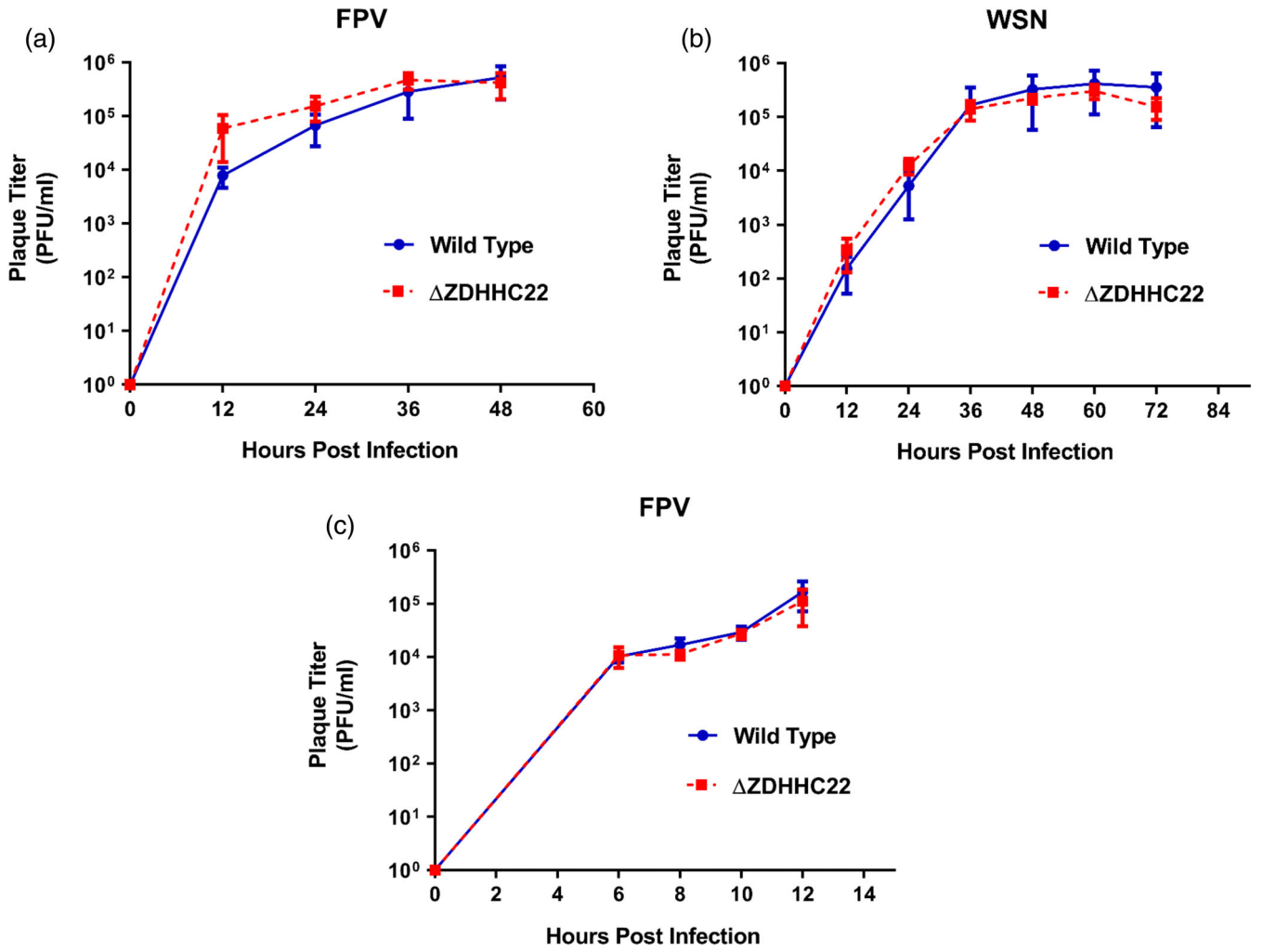

FIGURE 6 Growth curve of influenza viruses in wildtype and ΔZDHHC22 knockout cells. WT and ΔZDHHC22 A549 cells were infected with FPV M1 (a,c) or WSN (b) with an MOI of 0.01 (a, b), or 1 (c) and incubated at 37°C in medium containing 0.25 μg/ml TPCK-Trypsin. Aliquots of the cell culture supernatants were collected at indicated time points and the virus titers were determined by plaque assays in MDCKII cells. The data from three independent experiments are shown as mean including standard error. One-way ANOVA followed by Tukey's multiple comparison test showed that there was no statistically significant difference for any growth curve at any time point

almost identical, with a slight increase observed at early time points in ΔZDHHC22 cells, which is statistically significant for FPV at 12 hr post infection (Figure 6a,b). However, infection of cells with FPV M1 at a high MOI of 1 did not reveal a difference (Figure 6c). Thus, we conclude that the NS1-induced upregulation of ZDHHC22 does not affect replication of two Influenza A viruses in cell culture.

3 | DISCUSSION

In this study, we first analysed the expression pattern of members of the ZDHHC palmitoyl acyltransferase family in human lung cells. This is of interest since many viral pathogens that infect via the respiratory route contain at least one acylated membrane protein, but the responsible ZDHHCs have only yet been identified for HA of Influenza A virus. RT-PCR experiments show that every ZDHHC family member, with the exception of ZDHHC19, is expressed in uninfected A549 and Calu cell lines (Figure S1). This is largely consistent with data in the Human Protein Atlas, which revealed that every ZDHHC, except ZDHHC19 and ZDHHC22, has been detected in native human lung cells (Table S2). After infection with Influenza A virus we observed significant upregulation of ZDHHC22 expression in both cell lines, up to 30-fold if an avian strain was used for infection (Figure 1).

Since we assumed that ZDHHC22 might at least contribute to acylation of influenza virus proteins, we knocked out the *ZDHHC22* gene in A549 cells using CRISPR/Cas9 technology (Figure 3). However, neither acyl-RAC nor metabolic labeling revealed diminished acylation of HA and M2 of two Influenza A virus strains in ΔZDHHC22 cells (Figure 4). Mass spectrometry showed that these cells produced virus particles having a stoichiometrically acylated HA spike (Figure 5). Only a small increase in the amount of stearate (C18:0) relative to palmitate (more obvious in the case of WSN HA) was detected for virus collected from ΔZDHHC22 knockout cell line compared to wt A549 cells.

3.1 | Putative substrates of ZDHHC22

Using quantitative mass spectrometry, we identified 24 proteins that are acylated in A549 wt cells but not (or at greatly reduced levels) in ZDHHC22 knock-out cells, suggesting that these proteins are substrates of ZDHHC22. Besides a short isoform of ZDHHC18 (Morrison et al., 2015; Morrison et al., 2020), ZDHHC22 is the shortest member of the ZDHHC family, which is mainly localised in the ER/Golgi. Only two ZDHHC22 substrates have been identified so far, the large conductance calcium-activated potassium (BK) channel and the nephroblastoma overexpressed protein. In both cases palmitoylation is required for proper trafficking of the respective protein (Kim et al., 2018; Tian, McClafferty, Knaus, Ruth, & Shipston, 2012). Three of the proteins we identified, the regulatory subunit 16A of the protein phosphatase 1, the calcium sensor synaptotagmin 1, and the isoform 1 of plakophilin-2, were already described to be palmitoylated (Heindel, Schmidt, & Veit, 2003; Roberts et al., 2014). New substrates we identified include small GTPases and GTPase-activating proteins, protein kinases and phosphatases, transcriptional regulators and splicing factors, as well as proteins affecting the cytoskeleton and cell–cell adhesion (Table S6).

Our screen also identified another palmitoyl-transferase, ZDHHC13, as putative substrate of ZDHHC22. It is tempting to speculate that ZDHHC13 and ZDHHC22 are part of a palmitoylation cascade, similar to the one involved in acylation of ER-resident protein folding factors, where ZDHHC6 catalyses fatty acid transfer to the protein substrate, but its activity is regulated by ZDHHC16-catalysed palmitoylation of three cytoplasmic cysteines in ZDHHC6 (Abrami et al., 2017). Besides the cysteine in the DHHC motif, ZDHHC13 contains another cysteine located adjacent to the first transmembrane region, which might be the putative palmitoylation site. However, ZDHHC13 was also shown to regulate mitochondria architecture and function (Maynard et al., 2008; Shen et al., 2017) and to mediate palmitoylation-dependent magnesium transport into cells (Goytain, Hines, & Quamme, 2008). Interestingly, other proteins identified in our screen also localise to mitochondria (NADH–ubiquinone oxidoreductase chain 4) or are involved in magnesium transport (the metal transporter CNNM2).

The isoform 1 of plakophilin-2 is the only protein we identified that has been described to affect replication of Influenza A virus. In the nucleus it competes with the viral polymerase subunit PB2 for binding to the PB1 subunit. This perturbs assembly of a functional polymerase complex, thereby limiting polymerase activity and subsequent viral replication (Wang et al., 2017). In uninfected cells, plakophilin-2 binds to the cytoplasmic domain of cadherins, cell adhesion molecules of desmosomes at the plasma membrane, and palmitoylation at a single cysteine is important for desmosome assembly and hence cell–cell adhesion (Roberts et al., 2014). Whether palmitoylation affects the interaction of plakophilin-2 with the viral polymerase subunit has not been investigated. We report that expression of plakophilin-2 is barely detectable in ZDHHC22 knock-out cells and that these cells exhibit morphological changes, that is, are not able to form visible cell–cell contacts (Figure S4). We speculate that in the absence of ZDHHC22, plakophilin-2 is not palmitoylated, cannot induce the formation of desmosomes and is hence degraded.

To our knowledge none of the other ZDHHC22 or ZDHHC13 substrates has so far been linked to replication of Influenza virus. In general, palmitoylation of intrinsically hydrophilic substrates recruits the protein to certain cellular membranes, such that it can perform its function at a specific location. Palmitoylation of transmembrane proteins might have various functions, facilitating intracellular trafficking and recruitment to nanodomains in the membrane, promoting association with other proteins, or protecting from other post-translational modifications, such as ubiquitination thereby preventing degradation (Zaballa & van der Goot, 2018). Palmitoylation of many cellular proteins is reversible and thus the modification resembles phosphorylation, which is known to be involved in virus replication and evasion of the innate immune response (Meineke, Rimmelzwaan, & Elbahesh, 2019).

3.2 | Amino acids and functionalities in NS1 required for ZDHHC22 upregulation

We have also demonstrated that the viral protein NS1 is responsible for ZDHHC22 upregulation. It triggers ZDHHC22 expression in transfected cells, whereas recombinant viruses lacking a functional NS1 gene did not cause ZDHHC22 upregulation. From the NS1 proteins analysed here, NS1 from the avian FPV has the most pronounced effect on overexpression of ZDHHC22, both if NS1 was expressed from a plasmid and from the viral genome. However, since the antibody we used could not detect avian NS1 in transfected cells we cannot exclude that its stronger effect is due to a higher expression level and not an intrinsic property of the protein. NS1 from the human H1N1 viruses WSN and PR8, and also from the more recent Panama strain, also activate ZDHHC22 expression, but to a lesser extent (Figure 2).

NS1 has recently been described to induce the transcription of hundreds of cellular genes by "read through" transcription of polymerase II past the end of genes by global inhibition of transcription termination. The NS1 activity is a consequence of inhibiting the poly(A) sensing (PAS) subunit of the cleavage and polyadenylation specificity factor, CPSF30, since an Influenza virus H5N1 strain lacking the 73 C-terminal amino acids (including the CPSF30 binding site) does not induce readthrough transcription (Heinz et al., 2018). We therefore compared the CPSF30 binding site of FPV NS1 with the corresponding amino acids in the NS1 proteins which exhibit a weaker effect on upregulation of ZDHHC22. Figure 7a shows part of a crystal structure of a complex formed between zinc finger domains of CPSF30 and the C-terminal domain of NS1 from the human Udorn virus, which contains identical amino acids at the binding site as NS1 from FPV. Its core region comprises a highly conserved hydrophobic binding pocket in NS1 (labelled as cyan sticks), but two other conserved amino acids in NS1 (Phe103 and Met106) stabilise binding to CFSP30 (Das et al., 2008). These two residues are exchanged to Ser and Ile, respectively in NS1 of PR8, and as a consequence it does not bind to CFSP30 in vitro. Two other residues are substituted in NS1 of

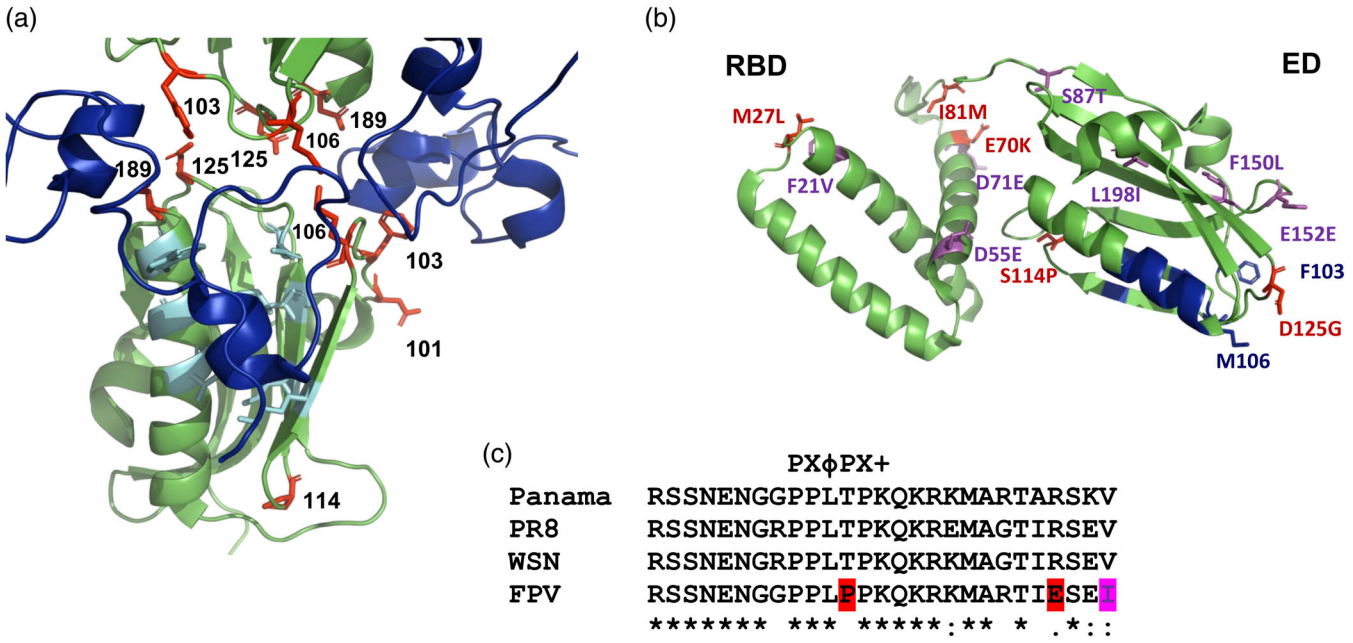

FIGURE 7 Structure of NS1 indicating amino acids present only in NS1 from FPV. (a) Detail of the structure of NS1 bound to the F2F3 fragment of human CPSF30. This crystal structure reveals an NS1:F2F3 tetrameric complex with two F2F3 binding pockets, but only one is depicted here. NS1 is shown as green and the F2F3 fragment as blue cartoons. The main hydrophobic pocket in NS1 for binding to CPSF30 is shown in cyan. Residues which are different between FPV NS1 and at least one of the other NS1 proteins are shown as red sticks. The figure was created with Pymol from PDB file 2RHK containing an NS1 protein from the influenza strain Udorn/307/1972, H3N2 (Das et al., 2008). (b) Structure of NS1 showing the amino acid differences between NS1 from FPV and from other NS1 proteins. The structure of a NS1 monomer is shown as a cartoon. The RNA-binding domain (RBD) is connected by a linker to the effector domain (ED). Residues which are present only in NS1 from FPV are shown as sticks, either coloured purple if they are exchanged by a similar amino acid or coloured red if they are exchanged by a non-similar amino acid in the other NS1 proteins analysed here. The main site in NS1 for binding to CFSP30 is coloured in blue. Two amino acids which modulate binding to CFSP30 (Phe 103, Met106) are shown as blue sticks. The figure was created with Pymol from PDB file 4OPH containing an NS1 protein from an avian H6N6 virus (Carrillo et al., 2014). (c) Amino acid sequence alignment at the C-terminus of NS1 proteins. Amino acids in NS1 of FPV not present in any of the other NS1s are highlighted in purple (conservative exchanges) and red (non-conservative exchanges), respectively. Pro is part of the Src-homology binding motif PXϕPX+ (Pro, any amino acid, hydrophobic, Pro, any amino acid, acidic), that is required for binding to the cellular Abl-kinase, which is not present in the other NS1 proteins

WSN: Asp189 is exchanged to Asn and Asp101 to His. The latter residue, which is close to the binding site, is exchanged to Asn in the Panama strain. Interestingly, two other residues at positions 114 and 125, which have been shown to affect binding to CFSP30 (Clark, Nogales, Martinez-Sobrido, Topham, & DeDiego, 2017; Rodriguez, Nogales, Iqbal, Perez, & Martinez-Sobrido, 2018), are exchanged in all three strains. Gly125 is exchanged by an acidic residue and Ser114 by a proline. Although residue 114 is quite remote from the binding site, Pro is known to cause a kink in the secondary structure of proteins which might indirectly affect the interaction with CFSP30. Thus, amino acid substitutions in the CFSP30 binding site might be partially responsible for the different activities of the NS1 proteins we tested. However, since NS1 from PR8 virus does not bind to CFSP30 but nevertheless activates expression of ZDHHC22 there might be other mechanisms involved.

NS1 is a multifunctional protein and interacts with several cellular proteins for which binding sites have been identified (Klemm et al., 2017; Krug, 2015; Marc, 2014). To get an idea which amino acids and hence binding partners might be responsible for the presumably stronger effect of the avian NS1, we aligned the NS1 sequences of the four investigated Influenza A viruses. We found 15 amino acids that are present in NS1 of FPV, but not in NS1 of any of the other strains investigated here; 12 of them are highlighted in the crystal structure of the molecule (Figure 7b), either as purple sticks (indicating conservative amino acid exchanges) or as red sticks (non-conservative exchanges). Five exchanges are located in the N-terminal RNA-binding domain, one affects a known SUMOylation site: position 70 is a Glu in NS1 of FPV, but a Lys in the human NS1 proteins, with only the latter being a potential SUMOylation acceptor site (Santos et al., 2013). Two amino acids are located in the between-strains variable linker region, which might affect the positioning of the RBD relative to the downstream effector domain. The remaining five amino acids are located in the effector domain; three are conservative exchanges that are unlikely to have a strong effect on the functionalities of NS1.

Three other exchanges are located in the intrinsically disordered C-terminus of NS1 (Hale, 2014), which is not present in the crystal structure: Ile230 is exchanged to Leu, Glu227 is exchanged to Arg and Pro215 is exchanged to Thr (Figure 7c). The latter is a known threonine phosphorylation site in the human NS1 proteins (Hutchinson et al., 2012). Interestingly, in FPV and other avian viruses Pro215 is

part of a second Src-homology binding motif, which is required for binding to and inhibition of the cellular kinase c-Abl that controls multiple signalling processes (Hrincius et al., 2014). Thus, inhibition of the cellular c-Abl kinase might be part of the mechanism responsible for the higher activity of NS1 from FPV.

In summary, it is reasonable to assume that NS1 activates overexpression of ZDHHC22 by two mechanisms: a basic, weakly effective mechanism that can be executed by many NS1 proteins and a more efficient mechanism in NS1 from FPV. The latter might involve inhibition of the cellular c-Abl kinase and/or binding to CFSP30. However, the physiological role of the upregulation of ZDHHC22 remains unclear, as infectious titers of two Influenza A viruses were not reduced in ΔZDHHC22 A549 epithelial cells. Since one main function of NS1 is the inhibition of the innate immune response, including the induction of the type I interferon production, the precise role of ZDHHC22 overexpression might become more evident under conditions that take into account the communication networks of an integrated immune response.

4 | EXPERIMENTAL PROCEDURES

4.1 | Cell culture and virus infection

Human lung epithelium cells A549, Calu-3 and MDCK-II cells were grown in Dulbecco's modified Eagle's medium (DMEM, PAN-Biotech) supplemented with 10% heat-inactivated fetal bovine serum at 37°C with 5% CO_2. Human influenza A/WSN/33 (H1N1) as well as a mutant of the highly pathogenic strain fowl plaque virus (FPV M1, A/chicken/*Rostock*/8/1934, H7N1) was used in the experiments, that contains the sequence PSKGR instead of PSKKRKKR at the C-terminus of HA1 (Wagner et al., 2013). This mutation creates a low pathogenic strain suitable for working in a BSL2 laboratory. Virus strains were propagated and titrated on MDCK-II cell line. ΔNS1 mutant influenza viruses (PR8 and Panama strains) are described in (Matthaei, Budt, & Wolff, 2013) and (Ludwig et al., 2002).

Cells were infected at multiplicity of infection (MOI) of 1. After 1 hr incubation with the virus, the inoculation media was replaced with pre-warmed infection media supplemented with 0.1% BSA and 1 μg/ml TPCK-trypsin and incubated at 37°C for 5 hr. To assess viral growth kinetics WT as well as ΔZDHHC22 A549 cells were inoculated with influenza viruses at a multiplicity of infection (MOI) of 0.01 plaque forming units (PFU). One hour post-infection, inoculum was removed and cells were washed with PBS and maintained in freshly prepared infection media (DMEM+0.1%BSA and 0.25 μg TPCK Trypsin) for virus replication. Viral supernatants were harvested at indicated time points and titers were determined by plaque assay in MDCK-II cells.

4.2 | Plasmids and antibodies

Viral cDNAs encoding the NS1 reading frames of the indicated IAV strains were integrated into the pCAGGS vector as described (Unterstab et al., 2005). The primary antibodies used in this study were rabbit anti-Hemagglutinin antibody (WSN strain) (1:3,000 dilution in 5% non-fat milk; Genetex, GTX127357), homemade rabbit anti-Hemagglutinin antibody (FPV strain) and homemade antibody against HA2 of FPV (1:3,000 dilution in 5% non-fat milk). Monoclonal mouse anti-influenza A NS1 (1:1,000 dilution in 5% non-fat milk, SC-130568, which was raised against recombinant NS1 protein of Influenza A/Puerto Rico/8/34. (H1N1) virus, with epitope mapping to the N-terminal domain). Mouse anti-Plakophilin-2 antibody, clone 8H6 (1:1,000 dilution in 5% non-fat milk, MABT394). Rabbit Anti-β-Actin (13E5) (1:1,000 dilution in 5% non-fat milk, #4970 Cell signalling). Mouse monoclonal anti-M2 antibody (1:2,000 dilution in 5% non-fat milk; abcam, ab5416) and mouse monoclonal anti-Flotillin-2 antibody (1:1,000 dilution in 5% non-fat milk; 610383, BD Biosciences). The secondary HRP antibodies (anti-rabbit, 1:5,000, abcam, ab191866 and anti-mouse, 1:2,000, Biorad, 1706516) both diluted in in 5% non-fat milk).

4.3 | RNA isolation and cDNA synthesis

Supernatants from virus-infected cells were removed, cells were scraped from the plate and pelleted by centrifugation. Total RNA from lysed cell pellets was extracted using the RNeasy® plus Mini Kit (Qiagen, Germany) according to the manufacturer's instructions. cDNA synthesis was carried out immediately after RNA purification using *High Capacity cDNA Reverse Transcription kit* (Applied Biosystems, USA). A 20 μl reaction contains 10 μl of ×2 RT mastermix and 10 μl RNA template (1.2 μg) under the following cycling conditions: 25°C for 10 min, 37°C for 120 min followed by 85°C for 5 min. RNA and cDNA concentrations were measured with Nanodrop, the latter was stored at −80°C until use.

4.4 | Quantitative PCR

Quantitative PCR was used to analyse changes in mRNA levels of ZDHHCs in uninfected and virus-infected or in untransfected versus transfected cells. PCR primer pairs (listed in Table S3) for each ZDHHC were selected to generate amplicons of 80–225 base pairs. All primer sets were designed to work at the same annealing temperatures to allow detection of all ZDHHCs within the same qPCR run. All primers were synthesised by *Integrated DNA Technologies* (IDT-DNA, BVBA, Belgium). A 10 μl PCR reaction consists of 5 μl 2xpowerUp SYBR green master mix (Applied Biosystems, USA), 400 nM of each primer and 100 ng cDNA template in a qPCR 96-well plate (Eurogentec, Belgium). Non-template controls were also included as an indicator for contamination. The cycling conditions were as follows: UDG (uracil-DNA glycosylase) activation step at 50°C for 2 min, followed by incubation at 95°C for 2 min to activate the Dual-lock™ DNA polymerase. Amplification was then performed on an Applied Biosystems 7,500 Fast Real-Time PCR machine using 40 cycles of denaturation at 95°C for 15 s and annealing and extension at 60°C

for 30 s. Following amplification, amplicon specificity and purity for each ZDHHC was confirmed by melting curve analysis. Relative expression values for each ZDHHC mRNA were normalised to human GAPDH, that is, the Ct-value obtained for GAPDH was subtracted from the Ct-value obtained for a ZDHHC (= ΔCt). The relative changes in ZDHHC expression levels were calculated by subtracting the ΔCt of uninfected or untransfected cells from infected or transfected cells and then using the following formula Fold Change = $2^{-\Delta\Delta Ct} = 2^{-(\Delta Ct \text{ of influenza infected} - \Delta Ct \text{ of Mock infected})}$. (Livak & Schmittgen, 2001).

4.5 | Generation of ZDHHC22 knockout cells with CRISPR/Cas9

Guide RNA (gRNA)-gene specific oligo sequences were selected to minimise the likelihood of off-target cleavage using the online MIT CRISPR and Atum gRNA designer tools (https://www.atum.bio/eCommerce/cas9/input). The sequence "ACCG" was added to the 5′ end of the gRNA-specifying oligonucleotide sequence and "AAAC" was added to the 5′ end of the reverse complement of the sgRNA-specifying oligonucleotide to allow cloning using the BsmBI restriction enzyme. The two oligonucleotides were then phosphorylated using the following conditions: gRNA forward oligo (10 μM); gRNA reverse complement oligo (10 μM); ×10 T4 ligation buffer and T4 polynucleotide kinase (5 units) (New England Biolabs) in a total volume of 20 μl for 1 hr at 37°C followed by inactivation at 65°C for 20 min. The phosphorylated oligonucleotides (10 μl each) were then annealed in 30 μl duplex buffer (60 mM HEPES pH 7.4 + 200 mM sodium acetate) at 95°C for 5 min; and then cooled down to 30°C at (0.01°C/sec) in a gradient PCR thermomixer.

The phosphorylated annealed oligonucleotides were cloned into pRP-418, a plasmid that expresses Flag-tagged Cas9, using Golden Gate cloning with the following conditions: 1 μg of circular pRP-418 vector is first digested by BsmBI restriction enzyme in NEB buffer 3.1 (×10) (New England Biolabs) at 55°C for 2 hr followed by enzyme inactivation at 80°C/20 min, Agarose gel electrophoresis and purification. Ligation of annealed oligonucleotides with linearized vector was carried out using T4 ligase under the following conditions: 100 ng BsmBI linearized pRP-418 vector, 1:10 Annealed oligos, T4 ligase; and T4 DNA ligase buffer (10x). 16°C/overnight. Ligation reaction was then transformed into Top10 competent cells. Colonies were picked and analysed for successful cloning using sequencing by U6 promoter specific sequencing primer (5′TTTGCTGTACTTTCTATAGTG′3).

To determine the lowest concentration of puromycin that kills 100% of non-transfected cells confluent cells were incubated with increasing concentrations of puromycin (0–5 μg/ml) for 5–7 days. For transfection cells were seeded in six well plates such that they reach 60–70% confluency the next day. Cells were transfected with the pRP-418 plasmid expressing single gRNA for the target gene as well as Cas9 nuclease using Lipofectamine 3,000 following manufacturer instructions (Thermo Scientific). Transfected cells were incubated in complete growth media for 48 hr followed by addition of puromycin selection media (2 μg/ml) and left until death of all non-transfected cells. After puromycin selection, the remaining single-cell clones were isolated by limiting dilution in 96 well plate / or by cell culture cloning cylinders. Single cell clones have been expanded and screened by PCR on genomic DNA using primers flanking Cas9 edit site.

4.6 | Palmitoylation assays

4.6.1 | Acyl-Resin assisted capture (Acyl-RAC)

Protein S-acylation was analysed by the Acyl-RAC assay as described (Werno & Chamberlain, 2015), with some modifications. Cells in a six well plate were washed with PBS 16 hr after infection, lysed in 500 μl buffer A (0.5% Triton-X100, 25 mM HEPES [pH 7.4], 25 mM NaCl, 1 mM EDTA, and protease inhibitor cocktail). Disulfide bonds were reduced by adding Tris (2-carboxyethyl) phosphin (TCEP, Carl Roth, HN95.2) to a final concentration of 10 mM and incubated at RT for 30 min. Free SH-groups were blocked by adding methyl methanethiosulfonate (MMTS, Sigma, 208,795, dissolved in 100 mM HEPES, 1 mM EDTA, 87.5 mM SDS) to a final concentration of 1.5% (v/v) and incubated for 4 hr at 40°C. Subsequently, 3 volumes of ice-cold 100% acetone was added to the cell lysate and incubated at −20°C overnight. Precipitated proteins were pelleted at 5,000 × g for 10 min at 4°C. Pelleted proteins were washed five times with 70% (v/v) acetone, air-dried, and then re-suspended in binding buffer (100 mM HEPES, 1 mM EDTA, 35 mM SDS). Twenty to thirty microlitre of the sample was removed to check for total protein expression by Western-blotting. The remaining lysate was divided into two equal aliquots. One aliquot was treated with hydroxylamine (0.5 M final concentration, added from a 2 M hydroxylamine stock adjusted to pH 7.4) to cleave thioester bonds. The second aliquot was treated with 0.5 M Tris–HCl pH 7.4. Thirty microlitre thiopropyl Sepharose beads (Sigma, T8387), which were beforehand activated by incubation for 15 min in aqua dest, were added at the same time to capture free SH-groups. Samples were incubated with beads overnight at room temperature on a rotating wheel. The beads were then washed 5x in binding buffer and bound proteins were eluted from the beads with ×2 non-reducing SDS-PAGE sample buffer for 5 min at 95°C. Samples were then subjected to SDS-PAGE and Western-blotting.

4.6.2 | Metabolic labeling with fatty acid analogue, immunoprecipitation and click chemistry

Wild type and ΔZDHHC22 A549 cells were infected at an MOI of 1 for 5 hr, then washed ×3 with serum free DMEM and incubated with the 17-ODYA fatty acid analogue (1:1,000) (Cayman chemicals) in DMEM supplemented with 5% dialyzed serum for 6 hr. For immunoprecipitation, cells were rinsed three times with cold PBS and lysed for 30 min at 4°C in IP-buffer (0.5% NP-40, 500 mM Tris pH 7.4, 20 mM EDTA, 10 mM NaF, 2 mM benzamidine and protease inhibitor cocktail). Cell lysates were centrifuged (5,000 × g for 5 min) and

supernatants were incubated with 20 μl of sepharose protein G beads (GE Healthcare) for 1 hr at 4°C. Cleared supernatants were incubated with viral antibodies (FPV-HA2) or WSN-HA and 20 μl protein G beads overnight at 4°C on a rotating wheel. Bound proteins were washed ×3 with IP-buffer and click chemistry reaction was done for 1 hr at room temperature (RT) using (1.25 Mm TAMRA Azide, 50 mM TCEP, 1x TBTA and 50 mM $CuSo_4$) (Martin, 2013). Click reaction was stopped by adding 4x sample loading buffer and boiled at 95°C 5 min. Proteins were subjected to SDS-PAGE and the fluorescence in the resulting gel was visualised with a Typhoon 9400 fluorescence scanner.

4.6.3 | SDS-PAGE and western-blot

After sodium dodecyl sulfate-polyacrylamide gel electrophoresis (SDS-PAGE) using 12% polyacrylamide, gels were electrophoretically transferred (200 mA for 1 hr) onto polyvinylidene difluoride (PVDF) membranes (GE Healthcare). After blocking (blocking solution: 5% skim milk powder in PBS with 0.1% Tween-20 [PBST]) for 1 hr at room temperature, membranes were incubated with the primary antibody overnight at 4°C. The following commercial antibodies were used: Influenza A virus H1N1 HA antibody from rabbit (Genetex, GTX127357, 1:3,000 dilution in 5% non-fat milk), Caveolin-1 (N-20) antibody from rabbit (Santa Cruz-894, 1:1,000) and anti-Influenza A Virus M2 protein monoclonal antibody 14C2 from mice (abcam, ab5416, 1:2,000). To detect H7 subtype HA we used our antiserum against the HA2 subunit of the FPV strain at a dilution of 1:3,000.

4.6.4 | MALDI-TOF MS analysis of HA in virus particles

Virus preparations were incubated with Iodoacetamide (30 mM final concentration, 1 hr in dark) before SDS-PAGE separation. Protein bands were electro-blotted onto PVDF membranes (Merck) and visualised by Ponceau S (Fluka) staining. The band corresponding to HA was cut from the membrane and subjected to trypsin in-gel hydrolysis as described in (Kordyukova, Krabben, Serebryakova, & Veit, 2019). Briefly, small membrane pieces were rinsed with 100–200 μl of 40% acetonitrile/50 mM $NH4HCO_3$ (pH 7.5) and digested with 5–10 μl of trypsin (Promega, 15 ng/μl in 80% acetonitrile/50 mM $NH4HCO_3$, pH 7.5) for 1–2 hr at 37°C. The reaction was stopped by adding a twofold volume of 0.5% trifluoroacetic acid. An aliquot (1–2 μl) of the water-acetonitrile solution containing hydrophilic and slightly hydrophobic peptides was used to confirm the protein identity by MALDI-TOF MS analysis and Mascot server (www.matrixscience.com) search. Strongly hydrophobic peptides were further extracted from the membrane pieces with a mixture (1:1, 10–20 μl) of hexafluoroisopropanol (HFIP) and chloroform for 2 hr to overnight. The water-acetonitrile and HFIP/chloroform extracts were combined, several μl of 0.5% trifluoroacetic acid was added to the solution until phase separation occurred, and the organic phase was collected for MALDI-TOF MS analysis. Sample aliquots (1 μl) were mixed on a steel target with an equal volume of 2,5-dihydroxybenzoic acid saturated solution in 30% acetonitrile/0.5% trifluoroacetic acid solution. Mass spectra were recorded on an UltrafleXtreme MALDI-TOF/TOF mass spectrometer (Bruker Daltonics, DE) equipped with an Nd laser. The MH+ molecular ions were detected in linear mode; the accuracy of mass peak measuring was within 0.01%. Matching of the peaks to the HA protein sequence was manually interpreted using GPMAW software (Lighthouse data, Denmark). The amount of stearate was calculated from the MS peak intensities using the method developed earlier (Serebryakova, Kordyukova, Baratova, & Markushin, 2006).

4.6.5 | Quantitative mass spectrometry and data analysis

Wild type and ΔZDHHC22 eluates of hydroxylamine treated ($+NH_2OH$) and untreated ($-NH_2OH$) acyl-RAC-enriched fractions were run on an SDS-PAGE gel and stained with Coomassie. Gel lanes were cut into 24 parallel bands of equal size. Bands from untreated samples were labelled with ^{16}O (light) and +HA bands with ^{18}O (heavy) via in-gel tryptic digestion, as previously described (Morrison et al., 2015). After deactivation of trypsin by acidification to pH ∼ 2.0 and heating to 95°C for 20 min, light and heavy peptide samples of corresponding bands were mixed, dried on a speed vac, and resuspended in 15 μl 0.1% (v/v) TFA and 5% (v/v) acetonitrile. 6.5 μl of this peptide mixture was injected onto a reversed-phase capillary nano liquid chromatography (LC) system (Ultimate 3,000, Thermo Scientific, USA) connected in-line to an Orbitrap Velos mass spectrometer (Thermo Scientific). Separation by LC was performed on a capillary column (Acclaim PepMap100 C18, 2 μm, 100 Å, 75 μm i.d. × 25 cm) at an eluent flow rate of 200 nl/min. The mobile phase A was composed of 0.1% formic acid in water, while the mobile phase B was 0.1% formic acid in acetonitrile. After pre-equilibration of the column with 3% mobile phase B, mobile phase B was linearly increased from 3% to 50% over 50 min. Mass spectra were measured in a data-dependent mode with a single MS survey scan, a m/z range of 350–1,500, an Orbitrap resolution of 60,000, and MS/MS scans of the 20 precursor ions with the highest intensities in the linear trap quadrupole. Two biological replicates were performed for each cell line. Raw files of each condition were searched together using Mascot Distiller (version 2.7.1.0) software against a custom database containing reviewed human proteins combined with influenza A virus (strain A/Wilson-Smith/1933-H1N1) proteins from Uniprot (accessed August 2017). The mass tolerance and sequence ion tolerance were set to 10 ppm and 0.35 Da, respectively. For quantification, only unique peptides identified better than homology were included, and proteins with fewer than two peptide heavy/light (H/L) ratios were filtered out. Filtered datasets of quantified protein ratios from all four replicates were then normalised by dividing all ratios by the median H/L ratio of each dataset and then combined.

ACKNOWLEDGEMENTS

The work was supported by a grant from the German Research Foundation to MV (Ve 141/18-1) and TW (TransRegio 84-B2), from the Russian Foundation for Basic Research to LK (20-54-12007).) C. F. was supported by the Deutsche Forschungsgemeinschaft (DFG, German Research Foundation) – Project-A05 – TRR 186 (278001972). The MALDI MS facility was made available in the framework of Moscow State University Development Program PNG 5.13. Open access funding enabled and organized by Projekt DEAL.

CONFLICT OF INTEREST

The authors declare no conflicts of interest.

AUTHOR CONTRIBUTIONS

Experiments were conducted and the data were analysed by Mohamed Rasheed Gadalla (Figures 1–4, Figure 6, Figures S2, S3 and S4), Xueijiao Han (Figure S1), Eliot Morrison (Table S6, supplemental data set), Marina V. Serebryakova (Figure 5) and Larisa Kordyukova (Figure 5). Michael Veit performed the structural analysis of NS1 (Figure 7). The same authors conceived and designed the respective experiments with input from Christian Freund (Table S6, supplemental data set), Michael Veit (Figures 1–4, Figure 6, Figures S2, S3 and S4) and Thorsten Wolff (Figure 2), who also supplied the NS1 clones and NS1-defective viruses. The manuscript was written by Michael Veit and Mohamed Rasheed Gadalla with input from all the other authors.

DATA AVAILABILITY STATEMENT

The data that supports the findings of this study are available in the manuscript, in the supplementary material and the supplementary data of this article.

ORCID

Michael Veit https://orcid.org/0000-0002-7638-1829

REFERENCES

Abrami, L., Dallavilla, T., Sandoz, P. A., Demir, M., Kunz, B., Savoglidis, G., … van der Goot, F. G. (2017). Identification and dynamics of the human ZDHHC16-ZDHHC6 palmitoylation cascade. *eLife*, *6*, 27826. https://doi.org/10.7554/eLife.27826

Brett, K., Kordyukova, L. V., Serebryakova, M. V., Mintaev, R. R., Alexeevski, A. V., & Veit, M. (2014). Site-specific S-acylation of influenza virus hemagglutinin: The location of the acylation site relative to the membrane border is the decisive factor for attachment of stearate. *The Journal of Biological Chemistry*, *289*(50), 34978–34989. https://doi.org/10.1074/jbc.M114.586180

Carrillo, B., Choi, J. M., Bornholdt, Z. A., Sankaran, B., Rice, A. P., & Prasad, B. V. (2014). The influenza a virus protein NS1 displays structural polymorphism. *Journal of Virology*, *88*(8), 4113–4122. https://doi.org/10.1128/JVI.03692-13

Castrucci, M. R., Hughes, M., Calzoletti, L., Donatelli, I., Wells, K., Takada, A., & Kawaoka, Y. (1997). The cysteine residues of the M2 protein are not required for influenza a virus replication. *Virology*, *238*(1), 128–134. https://doi.org/10.1006/viro.1997.8809

Chamberlain, L. H., & Shipston, M. J. (2015). The physiology of protein S-acylation. *Physiological Reviews*, *95*(2), 341–376. https://doi.org/10.1152/physrev.00032.2014

Chen, B. J., Takeda, M., & Lamb, R. A. (2005). Influenza virus hemagglutinin (H3 subtype) requires palmitoylation of its cytoplasmic tail for assembly: M1 proteins of two subtypes differ in their ability to support assembly. *Journal of Virology*, *79*(21), 13673–13684. https://doi.org/10.1128/JVI.79.21.13673-13684.2005

Clark, A. M., Nogales, A., Martinez-Sobrido, L., Topham, D. J., & DeDiego, M. L. (2017). Functional evolution of influenza virus NS1 protein in currently circulating human 2009 pandemic H1N1 viruses. *Journal of Virology*, *91*(17), 1–22. https://doi.org/10.1128/JVI.00721-17

Das, K., Ma, L. C., Xiao, R., Radvansky, B., Aramini, J., Zhao, L., … Montelione, G. T. (2008). Structural basis for suppression of a host antiviral response by influenza a virus. *Proceedings of the National Academy of Sciences of the United States of America*, *105*(35), 13093–13098. https://doi.org/10.1073/pnas.0805213105

Ernst, A. M., Syed, S. A., Zaki, O., Bottanelli, F., Zheng, H., Hacke, M., … Rothman, J. E. (2018). S-Palmitoylation sorts membrane cargo for anterograde transport in the Golgi. *Developmental Cell*, *47*(4), 479–493 e477. https://doi.org/10.1016/j.devcel.2018.10.024

Gadalla, M. R., Abrami, L., van der Goot, F. G., & Veit, M. (2020). Hemagglutinin of influenza a, but not of influenza B and C viruses is acylated by ZDHHC2, 8, 15 and 20. *Biochemical Journal*, *477*(1), 285–303. https://doi.org/10.1042/BCJ20190752

Gadalla, M. R., & Veit, M. (2019). Toward the identification of ZDHHC enzymes required for palmitoylation of viral protein as potential drug targets. *Expert Opinion on Drug Discovery*, *15*(2), 159–177. https://doi.org/10.1080/17460441.2020.1696306

Gamblin, S. J., Vachieri, S. G., Xiong, X., Zhang, J., Martin, S. R., & Skehel, J. J. (2020). Hemagglutinin structure and activities. *Cold Spring Harbor Perspectives in Medicine*., 1–19. https://doi.org/10.1101/cshperspect.a038638

Goytain, A., Hines, R. M., & Quamme, G. A. (2008). Huntingtin-interacting proteins, HIP14 and HIP14L, mediate dual functions, palmitoyl acyltransferase and Mg2+ transport. *The Journal of Biological Chemistry*, *283*(48), 33365–33374. https://doi.org/10.1074/jbc.M801469200

Grantham, M. L., Wu, W. H., Lalime, E. N., Lorenzo, M. E., Klein, S. L., & Pekosz, A. (2009). Palmitoylation of the influenza a virus M2 protein is not required for virus replication in vitro but contributes to virus virulence. *Journal of Virology*, *83*(17), 8655–8661. https://doi.org/10.1128/JVI.01129-09

Hale, B. G. (2014). Conformational plasticity of the influenza a virus NS1 protein. *The Journal of General Virology*, *95*(Pt 10), 2099–2105. https://doi.org/10.1099/vir.0.066282-0

Heindel, U., Schmidt, M. F., & Veit, M. (2003). Palmitoylation sites and processing of synaptotagmin I, the putative calcium sensor for neurosecretion. *FEBS Letters*, *544*(1–3), 57–62. https://doi.org/10.1016/s0014-5793(03)00449-6

Heinz, S., Texari, L., Hayes, M. G. B., Urbanowski, M., Chang, M. W., Givarkes, N., … Benner, C. (2018). Transcription elongation can affect genome 3D structure. *Cell*, *174*(6), 1522–1536 e1522. https://doi.org/10.1016/j.cell.2018.07.047

Hrincius, E. R., Liedmann, S., Anhlan, D., Wolff, T., Ludwig, S., & Ehrhardt, C. (2014). Avian influenza viruses inhibit the major cellular signalling integrator c-Abl. *Cellular Microbiology*, *16*(12), 1854–1874. https://doi.org/10.1111/cmi.12332

Hutchinson, E. C., Denham, E. M., Thomas, B., Trudgian, D. C., Hester, S. S., Ridlova, G., … Fodor, E. (2012). Mapping the phosphoproteome of influenza a and B viruses by mass spectrometry. *PLoS Pathogens*, *8*(11), e1002993. https://doi.org/10.1371/journal.ppat.1002993 PPATHOGENS-D-12-01111.

Kim, Y., Yang, H., Min, J. K., Park, Y. J., Jeong, S. H., Jang, S. W., & Shim, S. (2018). CCN3 secretion is regulated by palmitoylation via ZDHHC22. *Biochemical and Biophysical Research Communications*, *495*(4), 2573–2578. https://doi.org/10.1016/j.bbrc.2017.12.128

Klemm, C., Boergeling, Y., Ludwig, S., & Ehrhardt, C. (2017). Immunomodulatory nonstructural proteins of influenza a viruses. *Trends in Microbiology*, *26*(7), 624–636. https://doi.org/10.1016/j.tim.2017.12.006

Kordyukova, L., Krabben, L., Serebryakova, M., & Veit, M. (2019). S-acylation of proteins. *Methods in Molecular Biology*, *1934*, 265–291. https://doi.org/10.1007/978-1-4939-9055-9_17

Kordyukova, L. V., Serebryakova, M. V., Baratova, L. A., & Veit, M. (2009). Site-specific attachment of palmitate or stearate to cytoplasmic versus transmembrane cysteines is a common feature of viral spike proteins. *Virology*, *398*(1), 49–56. https://doi.org/10.1016/j.virol.2009.11.039

Krug, R. M. (2015). Functions of the influenza a virus NS1 protein in antiviral defense. *Current Opinion in Virology*, *12*, 1–6. https://doi.org/10.1016/j.coviro.2015.01.007

Kummer, S., Flottmann, M., Schwanhausser, B., Sieben, C., Veit, M., Selbach, M., … Herrmann, A. (2014). Alteration of protein levels during influenza virus H1N1 infection in host cells: A proteomic survey of host and virus reveals differential dynamics. *PLoS One*, *9*(4), e94257. https://doi.org/10.1371/journal.pone.0094257

Livak, K. J., & Schmittgen, T. D. (2001, Dec). Analysis of relative gene expression data using real-time quantitative PCR and the 2(-Delta Delta C[T]) method. *Methods*, *25*(4), 402–408. https://doi.org/10.1006/meth.2001.1262

Ludwig, S., Wang, X., Ehrhardt, C., Zheng, H., Donelan, N., Planz, O., … Wolff, T. (2002). The influenza a virus NS1 protein inhibits activation of Jun N-terminal kinase and AP-1 transcription factors. *Journal of Virology*, *76*(21), 11166–11171. https://doi.org/10.1128/jvi.76.21.11166-11171.2002

Marc, D. (2014). Influenza virus non-structural protein NS1: Interferon antagonism and beyond. *The Journal of General Virology*, *95*(Pt 12), 2594–2611. https://doi.org/10.1099/vir.0.069542-0

Martin, B. R. (2013). Nonradioactive analysis of dynamic protein palmitoylation. *Current Protocols in Protein Science*, *73*, 141511–141519. https://doi.org/10.1002/0471140864.ps1415s73

Matthaei, M., Budt, M., & Wolff, T. (2013). Highly pathogenic H5N1 influenza a virus strains provoke heterogeneous IFN-alpha/beta responses that distinctively affect viral propagation in human cells. *PLoS One*, *8*(2), e56659. https://doi.org/10.1371/journal.pone.0056659

Maynard, T. M., Meechan, D. W., Dudevoir, M. L., Gopalakrishna, D., Peters, A. Z., Heindel, C. C., … Lamantia, A. S. (2008). Mitochondrial localization and function of a subset of 22q11 deletion syndrome candidate genes. *Molecular and Cellular Neurosciences*, *39*(3), 439–451. https://doi.org/10.1016/j.mcn.2008.07.027

Meineke, R., Rimmelzwaan, G. F., & Elbahesh, H. (2019). Influenza virus infections and cellular kinases. *Viruses*, *11*(2). https://doi.org/10.3390/v11020171

Morrison, E., Kuropka, B., Kliche, S., Brugger, B., Krause, E., & Freund, C. (2015). Quantitative analysis of the human T cell palmitome. *Scientific Reports*, *5*, 11598. https://doi.org/10.1038/srep11598

Morrison, E., Wegner, T., Zucchetti, A. E., Alvaro-Benito, M., Zheng, A., Kliche, S., … Freund, C. (2020). Dynamic palmitoylation events following T-cell receptor signaling. *Communications Biology*, *3*(1), 368. https://doi.org/10.1038/s42003-020-1063-5

Ohno, Y., Kihara, A., Sano, T., & Igarashi, Y. (2006). Intracellular localization and tissue-specific distribution of human and yeast DHHC cysteine-rich domain-containing proteins. *Biochimica et Biophysica Acta*, *1761*(4), 474–483. https://doi.org/10.1016/j.bbalip.2006.03.010

Rana, M. S., Kumar, P., Lee, C. J., Verardi, R., Rajashankar, K. R., & Banerjee, A. (2018). Fatty acyl recognition and transfer by an integral membrane S-acyltransferase. *Science*, *359*(6372), eaao6326. https://doi.org/10.1126/science.aao6326

Roberts, B. J., Johnson, K. E., McGuinn, K. P., Saowapa, J., Svoboda, R. A., Mahoney, M. G., … Wahl, J. K., 3rd. (2014). Palmitoylation of plakophilin is required for desmosome assembly. *Journal of Cell Science*, *127*(Pt 17), 3782–3793. https://doi.org/10.1242/jcs.149849

Rodriguez, L., Nogales, A., Iqbal, M., Perez, D. R., & Martinez-Sobrido, L. (2018). Identification of amino acid residues responsible for inhibition of host gene expression by influenza a H9N2 NS1 targeting of CPSF30. *Frontiers in Microbiology*, *9*, 2546. https://doi.org/10.3389/fmicb.2018.02546

Rossman, J. S., Jing, X., Leser, G. P., & Lamb, R. A. (2010). Influenza virus M2 protein mediates ESCRT-independent membrane scission. *Cell*, *142*(6), 902–913. https://doi.org/10.1016/j.cell.2010.08.029

Santos, A., Pal, S., Chacon, J., Meraz, K., Gonzalez, J., Prieto, K., & Rosas-Acosta, G. (2013). SUMOylation affects the interferon blocking activity of the influenza a nonstructural protein NS1 without affecting its stability or cellular localization. *Journal of Virology*, *87*(10), 5602–5620. https://doi.org/10.1128/JVI.02063-12

Schneider, J., & Wolff, T. (2009). Nuclear functions of the influenza a and B viruses NS1 proteins: Do they play a role in viral mRNA export? *Vaccine*, *27*(45), 6312–6316. https://doi.org/10.1016/j.vaccine.2009.01.015

Serebryakova, M. V., Kordyukova, L. V., Baratova, L. A., & Markushin, S. G. (2006). Mass spectrometric sequencing and acylation character analysis of C-terminal anchoring segment from influenza a hemagglutinin. *European Journal of Mass Spectrometry*, *12*(1), 51–62. https://doi.org/10.1255/ejms.792

Shen, L. F., Chen, Y. J., Liu, K. M., Haddad, A. N. S., Song, I. W., Roan, H. Y., … Chen, Y. T. (2017). Role of S-Palmitoylation by ZDHHC13 in mitochondrial function and metabolism in liver. *Scientific Reports*, *7*(1), 2182. https://doi.org/10.1038/s41598-017-02159-4.

Siche, S., Brett, K., Moller, L., Kordyukova, L. V., Mintaev, R. R., Alexeevski, A. V., & Veit, M. (2015). Two cytoplasmic acylation sites and an adjacent hydrophobic residue, but no other conserved amino acids in the cytoplasmic tail of HA from influenza a virus are crucial for virus replication. *Viruses*, *7*(12), 6458–6475. https://doi.org/10.3390/v7122950

Sugrue, R. J., Belshe, R. B., & Hay, A. J. (1990). Palmitoylation of the influenza a virus M2 protein. *Virology*, *179*(1), 51–56 Retrieved from http://www.ncbi.nlm.nih.gov/entrez/query.fcgi?cmd=Retrieve&db=PubMed&dopt=Citation&list_uids=2219738

Thaa, B., Tielesch, C., Moller, L., Schmitt, A. O., Wolff, T., Bannert, N., … Veit, M. (2012). Growth of influenza a virus is not impeded by simultaneous removal of the cholesterol-binding and acylation sites in the M2 protein. *The Journal of General Virology*, *93*(Pt 2), 282–292. https://doi.org/10.1099/vir.0.038554-0

Tian, L., McClafferty, H., Knaus, H. G., Ruth, P., & Shipston, M. J. (2012). Distinct acyl protein transferases and thioesterases control surface expression of calcium-activated potassium channels. *The Journal of Biological Chemistry*, *287*(18), 14718–14725. https://doi.org/10.1074/jbc.M111.335547

Unterstab, G., Ludwig, S., Anton, A., Planz, O., Dauber, B., Krappmann, D., … Wolff, T. (2005). Viral targeting of the interferon-{beta}-inducing Traf family member-associated NF-{kappa}B activator (TANK)-binding kinase-1. *Proceedings of the National Academy of Sciences of the United States of America*, *102*(38), 13640–13645. https://doi.org/10.1073/pnas.0502883102

Veit, M., Klenk, H. D., Kendal, A., & Rott, R. (1991). The M2 protein of influenza a virus is acylated. *The Journal of General Virology*, *72*(Pt 6), 1461–1465. https://doi.org/10.1099/0022-1317-72-6-1461

Veit, M., & Siche, S. (2015). S-acylation of influenza virus proteins: Are enzymes for fatty acid attachment promising drug targets? *Vaccine*, *33*(49), 7002–7007. https://doi.org/10.1016/j.vaccine.2015.08.095

Wagner, R., Gabriel, G., Schlesner, M., Alex, N., Herwig, A., Werner, O., & Klenk, H. D. (2013). Protease activation mutants elicit protective immunity against highly pathogenic avian influenza viruses of subtype H7 in chickens and mice. *Emerging Microbes & Infections*, *2*(2), e7. https://doi.org/10.1038/emi2013.7

Wagner, R., Herwig, A., Azzouz, N., & Klenk, H. D. (2005). Acylation-mediated membrane anchoring of avian influenza virus hemagglutinin is essential

for fusion pore formation and virus infectivity. *Journal of Virology*, *79*(10), 6449–6458. https://doi.org/10.1128/JVI.79.10.6449-6458.2005

Wang, L., Fu, B., Li, W., Patil, G., Liu, L., Dorf, M. E., & Li, S. (2017). Comparative influenza protein interactomes identify the role of plakophilin 2 in virus restriction. *Nature Communications*, *8*, 13876. https://doi.org/10.1038/ncomms13876

Werno, M. W., & Chamberlain, L. H. (2015). S-acylation of the insulin-responsive Aminopeptidase (IRAP): Quantitative analysis and identification of modified Cysteines. *Scientific Reports*, *5*, 12413. https://doi.org/10.1038/srep12413

Zaballa, M. E., & van der Goot, F. G. (2018). The molecular era of protein S-acylation: Spotlight on structure, mechanisms, and dynamics. *Critical Reviews in Biochemistry and Molecular Biology*, *53*(4), 420–451. https://doi.org/10.1080/10409238.2018.1488804

Zurcher, T., Luo, G., & Palese, P. (1994). Mutations at palmitylation sites of the influenza virus hemagglutinin affect virus formation. *Journal of Virology*, *68*(9), 5748–5754 Retrieved from https://www.ncbi.nlm.nih.gov/pubmed/8057456

SUPPORTING INFORMATION

Additional supporting information may be found online in the Supporting Information section at the end of this article.

How to cite this article: Gadalla MR, Morrison E, Serebryakova MV, et al. NS1-mediated upregulation of ZDHHC22 acyltransferase in influenza a virus infected cells. *Cellular Microbiology*. 2021;23:e13322. https://doi.org/10.1111/cmi.13322